Interplay of mesoscopic and Kondo effects for transmission amplitude of few-level quantum dots

T. Hecht,[1] A. Weichselbaum,[1] Y. Oreg,[2] and J. von Delft[1]
[1]*Physics Department, Arnold Sommerfeld Center for Theoretical Physics and Center for NanoScience, Ludwig Maximilians University, 80333 Munich, Germany*
[2]*Department of Condensed Matter Physics, The Weizmann Institute of Science, Rehovot 76100, Israel*
(Received 27 April 2009; revised manuscript received 27 July 2009; published 29 September 2009)

The magnitude and phase of the transmission amplitude of a multilevel quantum dot is calculated for the mesoscopic regime of level spacing large compared to level width. The interplay between Kondo correlations and the influence by neighboring levels is discussed. As in the single-level case, the Kondo plateaus of magnitude and phase disappear with increasing temperature. At certain gate voltages, "stationary" points are found at which the transmission phase is independent of temperature. Depending on the mesoscopic parameters of the adjacent levels (such as relative sign and magnitude of tunneling matrix elements), the stationary points are shifted to or repelled by the neighboring level.

DOI: 10.1103/PhysRevB.80.115330 PACS number(s): 73.23.Hk, 73.63.Kv, 73.40.Gk

I. INTRODUCTION

In a remarkable series of experiments,[1–6] the Heiblum group has analyzed the complex transmission amplitude, $t_d = |t_d| e^{i\alpha}$, of a quantum dot embedded in an Aharonov-Bohm ring. In particular, by analyzing the Aharonov-Bohm oscillations of the conductance of such a ring, the dependence of both the magnitude and phase of the transmission amplitude, $|t_d|$ and α, were measured as a function of various parameters such as gate voltage V_g applied to the dot, temperature T, mean coupling strength to the leads Γ, etc.

The first two experiments in this series[1,2] dealt with large dots containing many (>100) electrons. The experiment by Yacoby *et al.*[1] showed that coherent transport through a quantum dot is possible despite the presence of strong interactions. The next experiments by Schuster *et al.*[2] generated tremendous interest because the behavior of the transmission phase showed a surprisingly "universal" behavior as function of gate voltage: the phase experienced a series of sudden jumps by $-\pi$ (phase lapses) between each pair of Coulomb blockade peaks in the conductance through the dot. This contradicted a naive expectation that the behavior of the transmission phase should depend on microscopic details of the dot such as the signs of the matrix elements coupling a given level to the left or right lead.

Subsequent experiments by Ji *et al.*,[3,4] performed on smaller dots containing tens of electrons, analyzed how the occurrence of the Kondo effect influences the transmission amplitude, and in particular its phase. For transmission at zero temperature through a *single* level, the Kondo effect causes the magnitude of the transmission amplitude to exhibit (as function of gate voltage) a plateau at the unitary limit ($|t_d|=1$). For this regime it had been predicted by Gerland *et al.*[7] that the phase should show a plateau at $\alpha=\pi/2$, a result very different from the universal behavior mentioned above. While the experiments of Ji *et al.* did yield deviations from the universal phase behavior, they did not verify the prediction of a $\pi/2$ Kondo plateau in the phase. With hindsight, the reason probably was that the experiments did not realize the conditions assumed in the calculations of Gerland *et al.*,[7] namely, transport through only a single level.

Truly "mesoscopic" behavior for the phase was observed only rather recently by Avinun-Kalish *et al.*,[5] in even smaller dots containing only a small (<10) number of electrons. For these, the mean level spacing δ was significantly larger than the average level width Γ, so that for any given gate voltage, transport through the dot is typically governed by the properties of only a single level, namely, that closest to the Fermi energies of the leads. When the number of electrons was increased beyond about 14, universal behavior for the phase was recovered. Consequently, it was proposed[5,8–13] that the universal behavior occurs whenever a quantum dot is large enough for that the ratio δ/Γ is sufficiently small ($\simeq 1$) that for any given gate voltage, typically more than one level contributes to transport.

The latest paper in this series, by Zaffalon *et al.*,[6] studied the transmission phase through a quantum dot in the "deep mesoscopic" regime $\delta/\Gamma \gg 1$, containing only one or two electrons. When this system was tuned into the Kondo regime, the transmission phase indeed did show the $\pi/2$ Kondo plateau predicted by Gerland *et al.*[7]

The experiments of Avinun-Kalish *et al.*,[5] which observed mesoscopic effects for the transmission phase through a small number of levels, and those of Zaffalon *et al.*,[6] which found characteristic signatures of the Kondo effect in the transmission phase through a single level, raise the following question: what type of phase behavior can arise in the deep mesoscopic regime from the interplay of (i) *random signs* for tunneling amplitudes of neighboring levels and (ii) the *Kondo effect* for individual levels? In the present paper, we address this question by studying spin-degenerate models of dots with 2 or 3 levels in the deep mesoscopic regime of $\delta/\Gamma \gg 1$. This is the regime relevant for the experiments of Zaffalon *et al.*[6] (for those of Ji *et al.*,[3,4] the ratio δ/Γ was presumably smaller than used here). Our goal is to provide a catalogue of the types of behavior that can occur in this regime and to illustrate how the characteristic transmission amplitude (magnitude and phase) depends on temperature as well as on the strength of the coupling to the leads.

This paper is organized as follows. In Sec. II we introduce our many-level model for the quantum dot system. We discuss the relation between the Aharonov-Bohm contribution to the linear conductance and the transmission amplitude

through the quantum dot. The latter can be expressed in terms of the local Green's function of the dot. We briefly present the technique used to calculate the latter, the numerical renormalization group method. In Sec. III we present our numerical results of both the phase and the magnitude of the transmission amplitude through a two- and three-level model in the regime $\delta/\Gamma \gg 1$. We discuss the T and Γ dependence of the transmission amplitude with focus on the influence on Kondo correlations. We study all relevant choices of the mesoscopic parameters given by the relative signs of the tunneling amplitudes of adjacent levels. The influence of neighboring levels is studied. It results not only in a phase lapse in Coulomb blockade valleys but also introduces a V_g asymmetry in the finite-temperature modulations of the Kondo plateaus. "Stationary" points of T and Γ independence are discussed. In the Appendix, we give a derivation of a formula for the Aharonov-Bohm contribution to the linear conductance through a multiterminal interferometer with open geometry, as used in the Heiblum group. This formula has been used in several publications including some of the present authors,[7,11,12] but its derivation had not been published before.

II. MODEL AND METHOD

In the experiments,[2–6] the temperature-dependent transmission amplitude through the quantum dot is extracted from the Aharonov-Bohm oscillations of the conductance in a multilead ring geometry. In the Appendix, which contains a figure depicting such a geometry, we show that this transmission amplitude can be expressed in terms of the equilibrium local Green's function of the dot tunnel-coupled only to *two* leads on its left and right side, without explicitly incorporating the other leads of the ring geometry in the calculation.

In this section we introduce a reduced model (called "double-slit model" in the Appendix), describing the latter situation of a spinful multilevel quantum dot coupled to two reservoirs and present the transmission formula derived in the Appendix. Further, we comment on the numerical renormalization group method, used to calculate the local Green's function.

A. Model Hamiltonian

The model Hamiltonian can be split into three parts,

$$H = H_{\mathrm{d}} + H_{\mathrm{l}} + H_{\mathrm{t}}, \tag{1a}$$

specifying the properties of the bare dot, the leads and the coupling between the two systems, respectively. For N spinful levels coupled to a left (emitter) and right (collector) lead, these terms are given by

$$H_{\mathrm{d}} = \sum_{j=1..N} \sum_{\sigma} \varepsilon_{dj} n_{dj\sigma} + \sum_{\{j\sigma\}\neq\{j'\sigma'\}} \frac{U}{2} n_{dj\sigma} n_{dj'\sigma'} \tag{1b}$$

$$H_{\mathrm{l}} = \sum_{a=L,R} \sum_{k\sigma} \varepsilon_k c^{\dagger}_{ak\sigma} c_{ak\sigma} \tag{1c}$$

$$H_{\mathrm{t}} = \sum_{j} \sum_{a=L,R} \sum_{k\sigma} (t^j_a c^{\dagger}_{ak\sigma} d_{j\sigma} + \mathrm{H.c.}). \tag{1d}$$

Dot creation operators for level j and spin $\sigma=\{\uparrow,\downarrow\}$ are denoted by $d^{\dagger}_{j\sigma}$, with $n_{dj\sigma}=d^{\dagger}_{j\sigma}d_{j\sigma}$, where $j=1\cdots N$ labels the levels in order of increasing energy ($\varepsilon_{dj}<\varepsilon_{dj+1}$). We use an inter and intralevel independent Coulomb energy $U>0$. The leads are assumed to be identical and noninteracting with a constant density of states per spin of $\rho=1/2D$, where the half-bandwidth $D=1$ serves as energy unit. Electrons in lead a are created by $c^{\dagger}_{ak\sigma}$. The local levels are tunnel-coupled to the leads, with real overlap matrix elements t^j_a that for simplicity we assume to be energy and spin independent. The resulting broadening of each level is given by $\Gamma_j=\Gamma_{jL}+\Gamma_{jR}$, with $\Gamma_{ja}=\pi\rho(t^j_a)^2$. Notation: we define $s_j=\mathrm{sgn}(t^j_L t^j_R t^{j+1}_L t^{j+1}_R)=\pm$. For example, matrix elements of same sign result in $s_j=+$, whereas one different sign yields $s_j=-$. We further define $s\equiv\{s_1,\cdots,s_{N-1}\}$, and use $\gamma=\{\Gamma_{1L},\Gamma_{1R},\cdots,\Gamma_{NL},\Gamma_{NR}\}/\Gamma$, with the mean level broadening $\Gamma=1/N\Sigma_j\Gamma_j$. We assume constant level spacing $\delta=\varepsilon_{dj+1}-\varepsilon_{dj}$. The local levels can be shifted in energy by a plunger gate voltage V_g, with $\varepsilon_{dj}=j\delta-(V_g+V_{g0})$, where $V_{g0}=\frac{N+1}{2}\delta+\frac{2N-1}{2}U$. This convention ensures that in case of maximal symmetry ($t^j_a=const.$ for all j,a), the system possesses particle-hole symmetry at $V_g=0$.

B. Transmission

In the Appendix we generalize a result of Bruder, Fazio, and Schoeller[14] to show that the Aharonov-Bohm contribution to the linear conductance through the multiterminal interferometer with open geometry with a multilevel quantum dot embedded in one arm (illustrated by figures in the Appendix) can be expressed as

$$G^{AB}(T) = \frac{e^2}{h} \sum_{\sigma} |T_u||t_{d\sigma}(T)| \cos\left(2\pi\frac{\Phi}{\Phi_0} + \phi_0 + \alpha_{\sigma}(T)\right). \tag{2}$$

Here $T_u=|T_u|e^{i\phi_0+i2\pi\Phi/\Phi_0}$ is the energy- and temperature-independent transmission amplitude through the upper reference arm including the Aharonov-Bohm contribution $2\pi\Phi/\Phi_0$ to the phase, where Φ is the magnetic flux enclosed by the interferometer arms and $\Phi_0=h/e$ is the flux quantum. The equilibrium Fermi function of the leads are denoted by f_0. The effective, temperature-dependent transmission amplitude $t_{d\sigma}(T)$ for a spin-σ electron through the lower arm including the quantum dot is given by

$$t_{d\sigma}(T) = \int dE \left(-\frac{\partial f_0(E,T)}{\partial E}\right) T_{d\sigma}(E,T) \equiv |t_{d\sigma}|e^{i\alpha_{\sigma}}, \tag{3}$$

where

$$T_{d\sigma}(E,T) = \sum_{jj'} 2\pi\rho t^j_L t^{j'}_R \mathcal{G}^R_{j\sigma,j'\sigma}(E,T). \tag{4}$$

Therefore, only local properties like the local retarded Green's function $\mathcal{G}^R_{j\sigma,j'\sigma}$ and the Fermi function of the leads

enter in the transmission amplitude through the quantum dot $t_{d\sigma}$ [Eq. (3)]. Thus, it suffices to evaluate the local Green's function for the model given in Eqs. (1) in equilibrium at temperature T. Since we do not consider the effects of a magnetic field in this paper, $\mathcal{G}^R_{j\sigma,j'\sigma}$ and all quantities derived from it, such as $t_{d\sigma}$, do not depend on the spin index σ. We will hence drop this index henceforth and denote the transmission amplitude per spin by $t_d \equiv |t_d| e^{i\alpha}$.

In the zero-temperature limit and in linear response, the dot produces purely elastic potential scattering between left and right leads, which can be fully characterized[15] by the eigenvalues $e^{i2\delta_\nu}$ ($\nu=b,d$) per spin of the S matrix, and the transformation $\left(\begin{smallmatrix}\cos\theta & \sin\theta\\ -\sin\theta & \cos\theta\end{smallmatrix}\right)$, that maps the left-right basis of lead operators onto the b-d eigenbasis of S. The transmission amplitude per spin through the dot then reads

$$t_d = -iS_{LR} = \sin(2\theta)\sin(\delta_b - \delta_d)e^{i(\delta_b+\delta_d)}, \tag{5}$$

where in general θ and δ_ν are all V_g dependent. The phase δ_ν is related by the Friedel sum rule[16] to the charge (per spin) $n_\nu = \delta_\nu/\pi$ extracted by the dot from effective lead ν. As V_g is swept, the transmission amplitude goes through zero whenever $n_b = n_d$ mod 1, and a phase lapse by π occurs. Equation (5) is useful for the special case of "proportional couplings," $t^j_L = \pm\lambda t^j_R$ with λ independent of j, in which the occupations $n_{b,d}$ take a simple form. Then the two effective leads b and d are the even and odd combinations of the left and right leads, respectively, with $\tan\theta = 1/\lambda$ independent of V_g. Then each level either couples to the even *or* the odd lead, and the occupations extracted from the leads are given by $n_{E,O} = \Sigma_{j\in E,O} n_{dj\sigma}$. Note that if all levels are coupled to the same effective lead [which is the case for $s=\{+\cdots+\}$], the other effective lead decouples, thereby reducing the computational complexity significantly.

C. Method

We calculate the local Green's function $\mathcal{G}^R$ needed for the transmission amplitude [Eqs. (3) and (4), respectively] using the numerical renormalization group method[17] (NRG), a well-established method for the study of strongly correlated impurity systems. For a review, see Ref. 18. The key idea of NRG is the logarithmic discretization of the conduction band with a discretization parameter $\Lambda > 1$. As a result, H_l is represented as a semi-infinite chain, where only the first site couples to the local level. The hopping matrix elements along the chain fall off exponentially like $\Lambda^{-(n-1)/2}$ with the site number n (energy scale separation). The NRG Hamiltonian can be solved iteratively by successively adding sites and solving the enlarged system, thereby increasing the energy resolution with each added site by a factor of $\Lambda^{1/2}$. The corresponding increase in Hilbert space is dealt with by a truncation strategy that keeps only the lowest N_{keep} states for the next iteration.

For the calculation of Im $\mathcal{G}^R$ we use the full density matrix NRG,[19,20] based on the only recently developed concept of a complete basis set within NRG.[21] The real part of $\mathcal{G}^R$ is obtained by Kramers-Kronig transformation. Improvement of the results is obtained by the self-energy representation, where the U-dependent part of the impurity self-energy $\Sigma(\omega) = U\frac{F^R(\omega)}{G^R(\omega)}$ is expressed by two correlation function,[22] which both are calculated with the full density matrix NRG.

III. RESULTS

In this section we present our results for the phase and magnitude of the transmission amplitude t_d through the quantum dot. The gate voltage V_g is swept over a range sufficiently large that the full occupation spectrum of the quantum dot is covered ranging from 0 to $2N$. The exact distribution of the couplings seems to play only minor role for the transmission amplitude. Therefore we choose left-right symmetric coupling in the cases where all $s_j = +$, reducing the computational effort significantly, since then the odd channel decouples.

In the regime of interest, the deep mesoscopic regime, the mean level spacing δ is much larger than the typical level widths Γ_j, $\delta/\Gamma \gg 1$. Therefore electrons enter the dot one by one when increasing the gate voltage. Transport thus occurs mainly through one level at a time; more precisely, it occurs through a linear combination of all levels, where in the mesoscopic regime the level closest to the Fermi energy dominates.[11]

The section is organized as follows: we first elucidate the basic properties of the transmission amplitude for the example of a two-level system. Varying temperature T (at fixed coupling Γ), or average coupling Γ (at fixed T), we study both possible choices $s=+$ and $s=-$, respectively. In order to analyze the interplay of $s=+$ and $s=-$, we then present data for a three-level system for all four possible combinations of $s=\{s_1,s_2\}$. Additionally, this has the advantage that for the middle level "boundary effects" (effecting the outermost levels) can be assumed to be eliminated, thus the behavior of the middle level can be viewed as representative of a generic level in a multilevel quantum dot in the deep mesoscopic regime.

Unless otherwise noted, we use $U=0.6$. In order to cover all relevant energy scales with reasonable computational effort, we usually use $\Lambda=3.2$ for the two-level model and $\Lambda=3.5$ in case of three levels. We checked that already by keeping $\sim$1000 states at each iteration, also for the two-channel calculations (that involve at least one $s_i=-$) the physical trends are captured qualitatively. Note that since the eigenvalues of the scattering matrix are given by $e^{i2\delta_\nu}$, the transmission phase α is defined modulo π. For clarity of the figures, curves showing α are shifted by multiples of π as convenient.

A. Two-level model

1. Temperature dependence

Figure 1 shows the transmission amplitude for both $s=+$ (a,b) and $s=-$ (c,d), for fixed dot parameters and various different temperatures. The mean level broadening is chosen to be $\Gamma/U=0.03$ in panels (a,c), and $\Gamma/U=0.08$ in panels (b,d). Therefore the (V_g-dependent) bare Kondo temperatures[23]

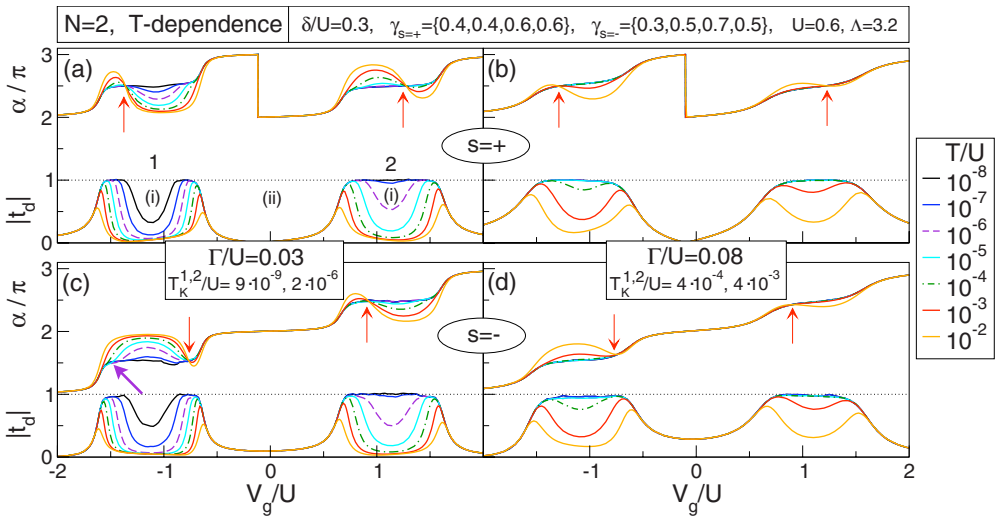

FIG. 1. (Color online) Transmission amplitude per spin, $t_d=|t_d|e^{i\alpha}$, through a spinful two-level quantum dot for various temperatures and constant couplings. Regimes (i), (ii), indicated in panel (a) only, refer to Kondo valleys or Coulomb blockade valleys, respectively (see text). The levels involved are indicated by their level number 1,2. Level 2 is coupled more strongly to the leads than level 1, resulting in different bare Kondo temperatures, e.g., $T_K^{j=1}<T_K^{j=2}$. We use $\Gamma/U=0.03$ (a,c) and $\Gamma/U=0.08$ (b,d), thus $T_K^{(a,c)}<T_K^{(b,d)}$. The minimum value of the T_K^j (in the center of the Kondo valleys) are indicated in the legends. In accordance with Ref. 24, we find shoulders in the phase [see, e.g., the fat arrow and the dashed curve $(T/U=10^{-6})$ in (c) for level 1] and an enhanced sensitivity of the phase to Kondo correlations compared to the magnitude, see e.g., the dashed-dotted $(T/U=10^{-4})$ curves in (d) for level 1 or the dashed curve $(T/U=10^{-6})$ for level 2 in (a). There, the typical $\frac{\pi}{2}$-Kondo plateau in the phase is present, whereas the Kondo plateau in amplitude is not fully developed yet. At certain points in gate voltage, say V_g^{cj} (as indicated by thin arrows), we find stationary points where the curves for α for all temperatures intersect. The position of V_g^{cj} is shifted by the presence of a neighboring level, being repelled by or shifted towards the latter for $s=+$ or $-$, compare (a,c) or (b,d), respectively. Depending on the mesoscopic parameter $s=\pm$, the phase either exhibits a sharp drop of π, accompanied by a zero in the amplitude $|t_d|$ [$s=+$, see (a,b)], or increases monotonically [$s=-$, see (c,d)] in the Coulomb blockade valleys.

$$T_K^j=\sqrt{\frac{\Gamma_j U}{2}}\exp\left[\pi\frac{\varepsilon_{dj}}{2U}\frac{(\varepsilon_{dj}+U)}{\Gamma_j}\right] \tag{6}$$

vary in a lower-lying range of energies for panels (a,c) than for panels (b,d). In all panels the relative coupling of the first and the second levels are chosen to be $\gamma=\{0.8,1.2\}$. Therefore, the bare Kondo temperature for level 1 is lower than for level 2, $T_K^{j=1}<T_K^{j=2}$, as indicated in the legends. The resulting difference in the temperature dependence can be nicely observed in the figure. We first describe those general properties of the transmission amplitude that qualitatively agree with those that one would obtain for just a single level, then discuss the effect of the presence of a second level.

a. General properties. In the mesoscopic regime, where transport mainly occurs through one level at a time, two different regimes of transmission can be distinguished as V_g is varied, as indicated in Fig. 1(a): These are (i) the Kondo valleys and (ii) the regime in between, to be called "Coulomb blockade valleys." There, the transmission amplitude is mainly determined by the mesoscopic parameter s, showing a phase lapse only in case $s=+$, similar for both spinful and spinless models.[11,12]

In the zero-temperature limit, $T\ll T_K^{(j)}$, the transmission amplitude exhibits the typical Kondo behavior: in the local-moment regime a typical Kondo plateau forms, with $|t_d|$ approaching the unitary limit, $|t_d|\to 1$. In the mixed valence regime the magnitude changes rapidly as a function of V_g. In the Coulomb blockade valleys, transmission is suppressed by Coulomb interaction. The transmission phase increases by $\sim\pi/2$ for each entering electron (see black curves for α in Fig. 1), increasing only slightly in between. In the Kondo valleys this results in a plateau at $\alpha \bmod \pi=\frac{\pi}{2}$, as direct consequence of the $\frac{\pi}{2}$ phase shift due to the formation of the Kondo singlet.

With increasing temperature, the Kondo effect is suppressed, thus the behavior in the middle of the Kondo valleys changes dramatically. The Kondo plateaus in $|t_d|$ and α disappear: The magnitude tends towards Coulomb blockade behavior, with a resonance of width $\sim\Gamma_j$ for each entering electron, while the phase develops a nonmonotonic V_g dependence. As in the single-level case, all finite-temperature curves of the phase intersect the zero temperature at the *same* gate voltage, say V_g^{cj} (see thin arrows). We shall refer to this gate voltage as a "stationary" point (with respect to temperature).

As observed in the experiments of Ji *et al.*[3] and emphasized by Silvestrov and Imry,[24] the transmission phase reacts more sensitively to the buildup of Kondo correlations with decreasing temperature than the transmission magnitude: α approaches its $T=0$ behavior already at temperatures $T\simeq T_K$ (the $\frac{\pi}{2}$ plateau develops), whereas $|t_d|$ develops its plateau for T significantly less than T_K [see the dashed-dotted curve $(T/U=10^{-4})$ for level 1 in Fig. 1(b) or the dashed curve $(T/U=10^{-6})$ for level 2 in Fig. 1(a)]. Similar to the predictions of Silvestrov and Imry,[24] we find shoulders in the evolution of the phase, see for example the fat arrow and the

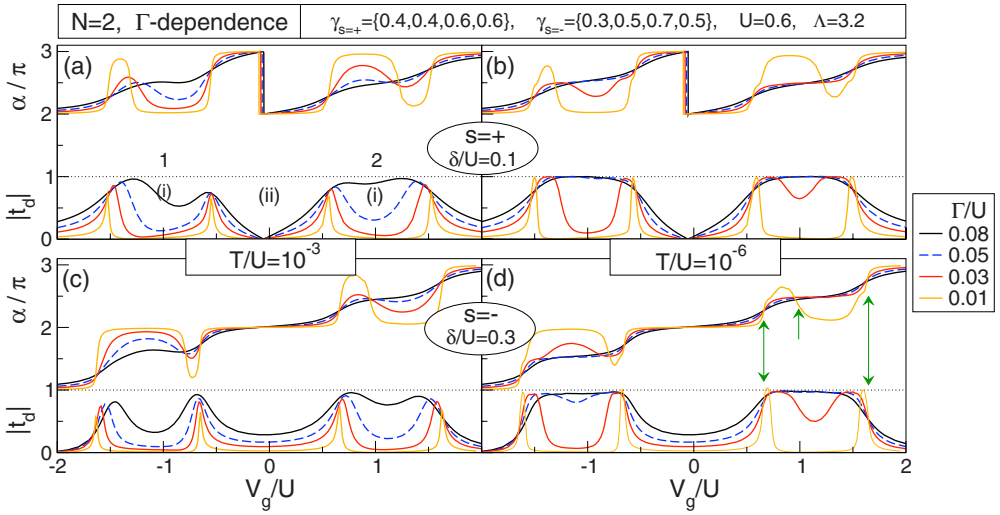

FIG. 2. (Color online) Transmission per spin through a spinful two-level quantum dot for both choices of $s=\pm$ and various values of mean couplings Γ at fixed temperature T, level spacing δ and relative couplings γ. Due to the mixing of the levels, no stationary points with respect to Γ exist, see text and the arrows in (d). Level numbers and the regime of (i) Kondo and (ii) Coulomb blockade valleys are indicated in panel (a) only.

dashed curve ($T/U=10^{-6}$) in Fig. 1(c). This indicates that the temperature is large enough to suppress Kondo correlations in the deep local-moment regime (middle of the Kondo valley), where T_K is very small. Towards the borders of the local-moment regime the crossover temperature for the onset of phase sensitivity increases [as does the Kondo temperature, see Eq. (6)], eventually exceeding the temperature. Then the phase tends towards its zero-temperature behavior, thus producing shoulders.

b. Properties special to the multilevel model. The most obvious difference between the transmission amplitude of the many-level model in the mesoscopic regime compared to the single-level model is the phase behavior in the Coulomb blockade valleys between the levels. Depending on s, i.e. on the relative sign of the tunnelling matrix elements of the two adjacent levels, the phase either exhibits a sharp drop ("phase lapse") by π in the $s=+$ case (accompanied by a transmission zero, $|t_d|=0$), or evolves continuously for $s=-$.[11,12,14,25–27] The phase lapse that occurs for $s=+$ is smeared out with increasing temperature [not discernible on the V_g scale used in Fig. 1, but evident, e.g., in Fig. 2(f) of Ref. 11 and in Fig. 4 of Ref. 12], allowing the phase lapse to be identified as such despite the fact that α is defined only modulo π. The phase lapse occurs already at zero temperature and also exists for spinless models,[11,12] contrary to the nonmonotonic phase evolution discussed above. Therefore, the relevant energy scale for the temperature dependence of this phase lapse is not related to the Kondo temperature but to the level distance and width of the effective transport levels.[24] It is therefore not a relevant energy scale in the temperature range studied in this work.

A further peculiarity for models with more than one level is the *asymmetry* (with respect to the center of the Kondo valleys) of the transmission amplitude in the local-moment regime at finite temperature, introduced by the mixing of neighboring levels. The asymmetry in phase can be characterized by the position of the stationary points, V_g^{cj} (indicted by thin arrows in Fig. 1). In case $s=+$, these points are repelled by the neighboring level, whereas they are shifted to the latter for $s=-$, compare for example Figs. 1(a) and 1(c) or Figs. 1(b) and 1(d). For $\Gamma_1 \neq \Gamma_2$, the repulsion and attraction is enhanced or reduced compared to $\Gamma_1=\Gamma_2$ for the level that is coupled less or more strongly to the leads, respectively. Clearly, in the limit of one decoupled level (effective one-level system), the stationary point of the other level is symmetric with respect to the corresponding Kondo plateau. The dips that form in the plateaus of the amplitude with increasing temperature develop a distinct asymmetry only for $T \gg T_K^{(j)}$, for which they tend to shift towards the corresponding V_g^{cj}. This is consistent with the fact that as the phase drop in the Kondo valley gets sharper with increasing temperature and approaches a quasiphase lapse, the magnitude experiences a minimum, as for every complex function. Interestingly, the asymmetry in phase is the same for all temperatures, thus already at temperature $T \lesssim T_K$ the phase "knows" in which direction (of V_g) the dip in magnitude will shift at higher temperatures.

2. Dependence on the coupling strength

In experiments, it is more convenient (and easier to control) to change the coupling strength between the quantum dot and the reservoirs than the temperature. Accordingly, Fig. 2 presents the transmission amplitude for various values of Γ, keeping the temperature constant. With decreasing Γ, the decrease in T_K together with the suppression of Kondo correlations is nicely illustrated. At fixed temperature $T > T_K$, the nonmonotonic V_g-dependence of the phase evolution gets more pronounced and sharper with decreasing Γ. In the Coulomb blockade valleys, the suppression of $|t_d|$ by Coulomb interaction increases with decreasing ration Γ/U.

In the single-level problem, in addition to stationary points with respect to temperature, we also find stationary

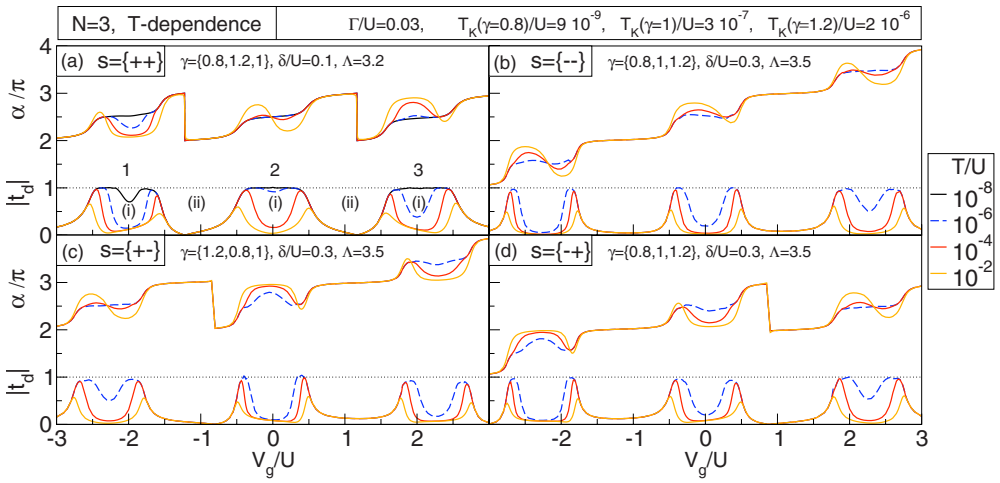

FIG. 3. (Color online) Transmission per spin through a three-level dot for all four possible combinations of $s=\{s_1,s_2\}$ and various temperatures, for fixed $\Gamma/U=0.03$. Level numbers and the regime of (i) Kondo and (ii) Coulomb blockade valleys are indicated in panel (a) only. The two-channel calculations for (b,c,d) qualitatively capture the physical trends. The asymmetry in the Kondo valleys is determined by both s and γ. For convenience the figure legends for γ display only the total relative coupling of each level. The minimal bare Kondo temperatures are indicated. (a) $s=++$: $\gamma=\{0.6,0.6,0.4,0.4,0.5,0.5\}$. The case $T/U=10^{-8}$ is included only for this panel. (b) $s=--$: $\gamma=\{0.5,0.3,0.4,0.6,0.5,0.7\}$. (c) $s=+-$: $\gamma=\{0.4,0.8,0.4,0.4,0.3,0.7\}$. (d) $s=-+$: $\gamma=\{0.5,0.3,0.3,0.7,0.7,0.5\}$.

points with respect to Γ for t_d, i.e., for magnitude and phase of the transmission amplitude. These occur at the outer flanks of the Kondo plateaus. Varying the mean coupling strength Γ at fixed γ, δ and T in the two-level model, as shown in Fig. 2, these points can still be recognized [indicated by arrows in (d)], even though the Γ independence is not perfect (within our numerical accuracy). We expect that due to the mixing of the levels, also the level distance δ has to be taken into account to recover these stationary points. Between the levels, near $V_g/U\approx 0$, another quasistationary point seems to occur.

B. Three-level model

Naturally, the question arises about the effects of several levels, with different choices of $s_i=\pm$, which is present only for models with more than two levels. Assuming that in the mesoscopic regime only neighboring levels mix significantly, i.e., simultaneously influence transport, any local level of a quantum dot (except the lowest or highest one) can be represented adequately by the middle level of a three-level model.

In Fig. 3 we present numerical data of a three-level model for all four possible combinations of $s=\{s_1,s_2\}$ and various temperatures. The second level is influenced by the effect of both s_1 and s_2, resulting in an effective enhancement or compensation of the asymmetry of the stationary point V_g^{c2} of level 2, as discussed in Sec. III A 1. Also the relative strength of the level couplings (given by γ) has to be considered. In Fig. 3(a), both s and γ symmetrize the transmission curves of the middle level, whereas in panel 3(b) γ shifts V_g^{c2} to positive V_g. In panels 3(c) and 3(d) both s and γ tend to increase the asymmetry.

Therefore, the transmission phase through a spinful quantum dot with Kondo correlations present has S-like shape in the local-moment regimes at $T\gg T_K$. Analogously to experiments, we find an asymmetry of this S-like shape. It is determined by both the relative strength γ and the sign s of the level couplings.

IV. CONCLUSION

In this paper, we present temperature-dependent NRG calculations of the magnitude and phase of the transmission amplitude through a multilevel quantum dot in the regime $\delta/\Gamma\gg 1$. Clearly, the Kondo correlations are suppressed with increasing temperature. The presence of neighboring levels results in a V_g asymmetry in the finite-temperature modulation of the Kondo valleys. The asymmetry depends on the relative signs of the tunneling matrix elements as well as on the relative couplings of the adjacent levels. Further, sharp phase lapses may occur between the levels. Studying a three-level model, the middle level can be understood as a representative of a generic level in a multilevel quantum dot.

Throughout the paper, we deliberately focussed only on the deep mesoscopic regime, for which the results can be understood rather straightforwardly. The crossover into the regime $\delta/\Gamma\simeq 1$, which is certainly of interest too in order to understand the fate of Kondo physics in the universal regime, and which we believe to be the regime relevant for the experiments of Ji *et al.*,[3,4] will be left as a subject for future studies.

ACKNOWLEDGMENTS

We acknowledge helpful discussions with Moty Heiblum, Michele Zaffalon, Vitaly Golovach, Assaf Carmi, and Michael Pustilnik. This research was supported in part by the DFG through Grants No. De-730/3-2, No. SFB631, and No. SFB-TR12, by DIP-H.2.1, and by the National Science Foundation under Grant No. NSF PHY05-51164. Financial support of the German Excellence Initiative via the "Nano-

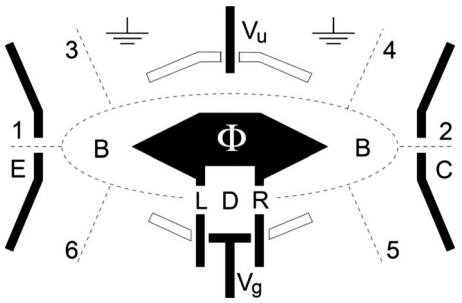

FIG. 4. Schematic depiction of an Aharonov-Bohm interferometer of the type used by the Heiblum group (compare Fig. 1 of Ref. 2): The base region (B), emittor (E), and collector (C) have chemical potentials $\mu_0=0$, μ_1, and μ_2, respectively. In the base region four reflectors (shown in white) and a central barrier (black) define an upper and lower arm forming a "ring" threaded by an applied magnetic flux Φ. The lower arm contains a quantum dot (D), coupled to the base region via tunable left and right tunnel barriers (L,R). The gate voltages V_g or V_u can be used to sweep the dot's energy levels relative to μ_0 or to change the transmission amplitude of the upper arm, respectively. The dashed lines are guide for the eyes, indicating how this devices realizes the geometry depicted in Fig. 5.

systems Initiative Munich (NIM)" is gratefully acknowledged.

APPENDIX: CONDUCTANCE FORMULA FOR MULTITERMINAL GEOMETRY

1. General case

We generalize the current formula derived by Bruder, Fazio, and Schoeller[14] for a single-level quantum dot embedded into one arm of an Aharonov-Bohm interferometer with two-terminal geometry to a multiterminal geometry with a multilevel dot, as used by the Heiblum group.[2–6] Fig. 4 shows a schematic depiction of the typical device layout used (adapted from Fig. 1 of the pioneering experiment;[2] the layout in subsequent experiments was similar in spirit, see, for example, Fig. 1 of Ref. 6). The derivation below will refer to an abstract depiction of the same geometry, shown in Fig. 5.

Consider a N-level quantum dot described by $H_{\rm d}$ [Eq. (1b)] embedded in one arm of an Aharonov-Bohm interferometer connected to six leads, as depicted in Fig. 5. Each lead, and each arm connecting them, is assumed to support only one mode. (This assumption is needed below only for arms 1 and 2 representing emittor and collector, respectively; it can be relaxed for arms 3 to 6 forming the base region, but will be retained here for notational simplicity.) The tunnelling between the local levels $j=1,\cdots,N$ on the quantum dot and the leads $\alpha=1,\cdots,6$ is described by

$$H_{\rm t}^{\rm multilead}=\sum_{j\sigma}\sum_{\alpha\epsilon}t^{j}_{\varepsilon\alpha\sigma}c^{\dagger}_{\alpha\varepsilon\sigma}d_{j\sigma}+\text{H.c.} \tag{A1}$$

Here $t^{j}_{\varepsilon\alpha\sigma}$ is the amplitude (indicated by dashed arrow in Fig. 5) for an electron with spin σ, initially in dot state $|j\sigma\rangle$, to tunnel off the dot and end up with energy ε in lead α, represented by lead state $|\varepsilon\alpha\sigma\rangle$. Since it can tunnel off to the left or the right, this amplitude can be represented as $t^{j}_{\varepsilon\alpha\sigma}=\Sigma_{a=L,R}t^{j}_{a\sigma}A^{a}_{\varepsilon\alpha}$, where $t^{j}_{a\sigma}=\langle x_a\sigma|j\sigma\rangle$ is the amplitude (chosen to be real) to get from dot state $|j\sigma\rangle$ to point x_a on side $a=L,R$ of the dot (solid arrow), and $A^{a}_{\varepsilon\alpha}=\langle\varepsilon\alpha\sigma|x_a\sigma\rangle$ is the amplitude (assumed spin independent) to get from point x_a to lead state $|\varepsilon\alpha\sigma\rangle$ without traversing the dot (dashed-dotted arrow).

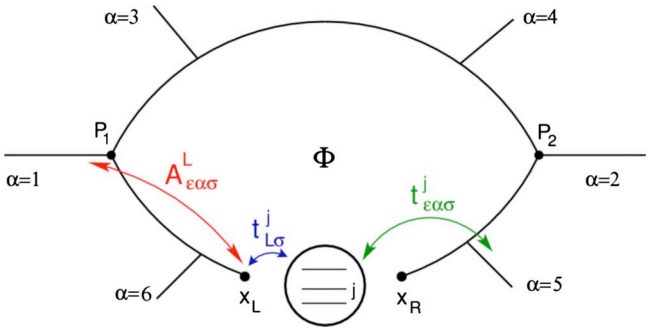

FIG. 5. (Color online) Abstract depiction of a multiterminal Aharonov-Bohm interferometer, with a multilevel quantum dot embedded in the lower arm, penetrated by a magnetic flux Φ. The different tunnelling amplitudes used in the text are indicated by arrows.

Following Büttiker,[28] the current operator in reservoir α is given by

$$\hat{I}_{\alpha}(t)=\frac{e}{h}\sum_{\varepsilon\varepsilon'}\sum_{\sigma\sigma'}\frac{1}{\rho}[c^{\dagger}_{\varepsilon'\alpha\sigma'}(t)c_{\varepsilon\alpha\sigma}(t)-b^{\dagger}_{\varepsilon'\alpha\sigma'}(t)b_{\varepsilon\alpha\sigma}(t)], \tag{A2}$$

where ρ, the density of states per spin, is assumed to be constant and equal for each reservoir. The first term inside the bracket stands for the incident, the second term for the reflected current in reservoir α, thus $b_{\varepsilon\alpha\sigma}=\Sigma_{\beta}S^{\varepsilon}_{\alpha\beta}c_{\varepsilon\beta\sigma}$, with $S^{\varepsilon}_{\alpha\beta}$ the (spin independent) scattering amplitude to get from lead β to lead α with energy ε. Defining the lesser, retarded, and advanced correlation functions

$$\mathcal{G}^{<}_{\mu,\mu'}(t-t')\equiv\frac{i}{\hbar}\langle a^{\dagger}_{\mu'}(t')a_{\mu}(t)\rangle=\int\frac{dE}{2\pi\hbar}e^{-iE(t-t')/\hbar}\mathcal{G}^{<}_{\mu,\mu'}(E), \tag{A3}$$

$$\mathcal{G}^{R,A}_{\mu,\mu'}(t-t')\equiv-\frac{i}{\hbar}\theta(\pm(t-t'))\langle[a^{\dagger}_{\mu'}(t'),a_{\mu}(t)]_{+}\rangle$$

$$=\int\frac{dE}{2\pi\hbar}e^{-iE(t-t')/\hbar}\mathcal{G}^{R,A}_{\mu,\mu'}(E), \tag{A4}$$

where a_{μ} denotes a fermionic operator with composite index μ, the expectation value of the current operator Eq. (A2)can be expressed as

$$\langle\hat{I}_{\alpha}\rangle=\frac{e}{h}\sum_{\varepsilon\varepsilon'}\sum_{\beta\beta'}\sum_{\sigma\sigma'}\frac{1}{\rho}[\delta_{\alpha\beta'}\delta_{\alpha\beta}-S^{\varepsilon'*}_{\alpha\beta'}S^{\varepsilon}_{\alpha\beta}]$$

$$\times(-i)\int\frac{dE}{2\pi}\mathcal{G}^{<}_{\varepsilon\beta\sigma,\varepsilon'\beta'\sigma'}(E). \tag{A5}$$

To calculate $\mathcal{G}^<(E)$ in Eq. (A5), we use the standard Dyson equation for the Keldysh 2×2 matrix Green's function[29] $\hat{\mathcal{G}}(E)$,

$$\hat{\mathcal{G}}_{\varepsilon\alpha\sigma,\varepsilon'\alpha'\sigma'}(E) = \delta_{\varepsilon\varepsilon'}\delta_{\alpha\alpha'}\delta_{\sigma\sigma'}\hat{\mathcal{G}}^0_{\varepsilon\alpha\sigma}(E) + \sum_{jj'} \hat{\mathcal{G}}^0_{\varepsilon\alpha\sigma}(E) t^j_{\varepsilon\alpha\sigma} \hat{\mathcal{G}}^d_{j\sigma,j'\sigma'}(E) t^{j'*}_{\varepsilon'\alpha'\sigma'} \hat{\mathcal{G}}^0_{\varepsilon'\alpha'\sigma'}(E), \tag{A6}$$

which yields

$$\mathcal{G}^<_{\varepsilon\alpha\sigma,\varepsilon'\alpha'\sigma'}(E) = \delta_{\varepsilon\varepsilon'}\delta_{\alpha\alpha'}\delta_{\sigma\sigma'}\mathcal{G}^{0<}_{\varepsilon\alpha\sigma}(E) + \sum_{jj'} t^j_{\varepsilon\alpha\sigma}[A+B+C] t^{j'*}_{\varepsilon'\alpha'\sigma'}, \tag{A7}$$

where terms in square brackets are given by

$$A = \mathcal{G}^{0R}_{\varepsilon\alpha\sigma}(E)\mathcal{G}^<_{j\sigma,j'\sigma'}(E)\mathcal{G}^{0A}_{\varepsilon'\alpha'\sigma'}(E),$$

$$B = \mathcal{G}^{0R}_{\varepsilon\alpha\sigma}(E)\mathcal{G}^R_{j\sigma,j'\sigma'}(E)\mathcal{G}^{0<}_{\varepsilon'\alpha'\sigma'}(E),$$

$$C = \mathcal{G}^{0<}_{\varepsilon\alpha\sigma}(E)\mathcal{G}^A_{j\sigma,j'\sigma'}(E)\mathcal{G}^{0A}_{\varepsilon'\alpha'\sigma'}(E),$$

and the free Green's functions for the leads have the form

$$\mathcal{G}^{0R,A}_{\varepsilon\alpha\sigma}(E) = \frac{1}{E-\varepsilon\pm i0^+}, \tag{A8}$$

$$\mathcal{G}^{0<}_{\varepsilon\alpha\sigma}(E) = 2\pi i f_\alpha(E)\delta(\varepsilon - E), \tag{A9}$$

with $f_\alpha(E)$ the Fermi function of lead α. Inserting $\mathcal{G}^<$ [Eq. (A7)] into Eq. (A5), the current can be written as

$$\langle \hat{I}_\alpha\rangle = I^0_\alpha + \delta I_\alpha. \tag{A10}$$

I^0_α arises from the first term of Eq. (A7). It describes the situation when the dot is completely decoupled ($t^j_{\varepsilon\alpha\sigma}=0$), thus does not contribute to Aharonov-Bohm oscillations. The influence of the quantum dot on the Aharonov-Bohm oscillations is caused by δI_α, arising from the second expression of Eq. (A7). The energy sums $\Sigma_{\varepsilon\varepsilon'}$ in Eq. (A5) can be evaluated using the Kramers-Kronig relation

$$\sum_\varepsilon \frac{1}{\rho}\frac{S^\varepsilon}{E-\varepsilon\pm i0^+} = \begin{cases} -2\pi i S^E \\ 0 \end{cases}, \tag{A11}$$

where S^ε stands for $t^j_{\varepsilon\alpha\sigma}$ or $t^j_{\varepsilon\alpha\sigma}S^\varepsilon_{\alpha\beta}$, and the plus (minus) refers to the upper (lower) case, respectively. This relation follows from the fact that the amplitudes $t^j_{\varepsilon\alpha\sigma}$ and $S^\varepsilon_{\alpha\beta}$ have to be analytic in the upper half plane, in order to ensure that the full S matrix of the system (in the presence of tunneling), of which they are ingredients, satisfies the necessary causality requirements in the time domain.[30]

The two contributions to the current then read

$$I^0_\alpha = \frac{e}{h}\int dE \sum_\sigma \sum_\beta [\delta_{\alpha\beta} - |S^E_{\alpha\beta}|^2] f_\beta(E), \tag{A12a}$$

$$\delta I_\alpha = \frac{e}{h}\int \frac{dE}{2\pi}\sum_{\beta\beta'}\sum_{jj'}\sum_{\sigma\sigma'}[\delta_{\alpha\beta'}\delta_{\alpha\beta} - S^{E*}_{\alpha\beta'}S^E_{\alpha\beta}] \times (2\pi)^2\rho t^j_{E\alpha\sigma} t^{j'*}_{E\alpha'\sigma'}(-i)[\mathcal{G}^<_{j\sigma,j'\sigma'}(E) + \mathcal{G}^R_{j\sigma,j'\sigma'}(E) f_{\beta'}(E) - \mathcal{G}^A_{j\sigma,j'\sigma'}(E) f_\beta(E)]. \tag{A12b}$$

The expression for δI_α can be simplified somewhat by exploiting the relations

$$\mathcal{G}^{R/A}_{j\sigma,j'\sigma'}(E) = [\mathcal{G}^{A/R}_{j'\sigma',j\sigma}(E)]^*, \tag{A13a}$$

$$\mathcal{G}^<_{j\sigma,j'\sigma'}(E) = -\mathcal{G}^{<*}_{j'\sigma',j\sigma}(E) \tag{A13b}$$

and relabeling $(j\alpha\sigma)\leftrightarrow(j'\alpha'\sigma')$ in some terms, with the result:

$$\delta I_\alpha = \frac{e}{h}\mathrm{Re}\left\{\int dE \sum_{\beta\beta'}\sum_{jj'}\sum_{\sigma\sigma'}[\delta_{\alpha\beta'}\delta_{\alpha\beta} - S^{E*}_{\alpha\beta'}S^E_{\alpha\beta}] \times 4\pi\rho t^j_{E\beta\sigma} t^{j'*}_{E\beta'\sigma'}(-i) \times \left[\frac{1}{2}\mathcal{G}^<_{j\sigma,j'\sigma'}(E) + \mathcal{G}^R_{j\sigma,j'\sigma'}(E) f_{\beta'}(E)\right]\right\}. \tag{A14}$$

This is the desired generalization of Bruder, Fazio, and Schoeller.[14]

2. Simplifications

For the experimental setup used by Schuster *et al.*[2] (and equivalently for the ensuing papers)[3–6] to measure transmission phase shifts, two simplifying assumptions can be made. The first allows us to neglect nonequilibrium effects, the second to perform NRG calculations for a simplified in which the dot is coupled only to two leads.

a. Neglect of nonequilibrium effects

In the experimental setup used by Schuster *et al.*,[2] the leads $\alpha=3,4,5$, and 6 serve as draining reservoirs (to prevent multiple traversals of the ring, see below), and are all kept at the same chemical potential, $\mu_\alpha=\mu_0$. [We shall take $\mu_0=0$, but nevertheless display μ_0 explicitly in the discussion up to and including Eq. (A16).] This also fixes the chemical potential of the ring, referred to as "base region" in Ref. 2, to equal μ_0. Lead 1 and 2 serve as emitter and collector, respectively (see Fig. 4), with chemical potentials μ_1 and μ_2, and Fermi functions $f_{1,2}(E)=f_0(E-\mu_{1,2})$. A crucial feature of the device design depicted in Fig. 4 is that the point contacts between emitter or collector and the base region (marked P_1 and P_2 in Fig. 5) are so small that the voltage drops occur directly at these point contacts, and *not* at the tunnel barriers coupling the dot to the ring. Thus, while the emitter injects electrons into the base region from one side and the collector extracts them on the other side, thereby driving a small current, we may assume that this happens at a sufficiently small rate that the base region is not driven out of equilibrium. In other words, *we may assume that the dot*

and the ring to which it is tunnel-coupled, and also electrodes 3, 4, 5, and 6, are all in equilibrium (governed by μ_0*)* with each other. This implies that the dot Green's functions $\mathcal{G}^{R,A,<}_{j\sigma,j'\sigma'}(E)$ do not depend on μ_1 and μ_2 at all, and that they can be calculated using equilibrium methods, with chemical potential set by μ_0. [Note that presence of an equilibrium base region separating the dot from the emitter and collector makes this situation different from most experiments on transport through quantum dots, for which emitter and collector are directly adjacent to the dot, separated from it by tunneling contacts across which the voltage drops occur. In such cases, $\mathcal{G}^{R,A,<}_{j\sigma,j'\sigma'}(E)$ *do* depend on μ_1 and μ_2, and have to be computed using nonequilibrium methods.] Thus, for the present situation the lesser function can be expressed in terms of the retarded and advanced ones using the following standard equilibrium relation:

$$\mathcal{G}^{<}_{j\sigma,j'\sigma'}(E) = -f_0(E-\mu_0)[\mathcal{G}^{R}_{j\sigma,j'\sigma'}(E) - \mathcal{G}^{A}_{j\sigma,j'\sigma'}(E)]. \tag{A15}$$

The conductance in the linear response regime can be obtained by taking $\mu_1-\mu_2=eV$, where $e=|e|$, e.g., by setting[34]

$$\mu_1 = \mu_0 = 0, \quad \mu_2 = -eV, \tag{A16}$$

and calculating $G=\partial I_1/\partial V$, with I_1 given by Eq. (A14).

b. Reduction to a double-slit geometry

The reason why a multilead geometry was used in experiment is to avoid phase rigidity: in an Aharonov-Bohm ring connected to only two leads, current conservation and time-reversal symmetry imply, via Onsager-Casimir relations,[31] that the transmission phase of the dot does not vary smoothly with gate voltage, but can assume only two distinct values, differing by π. A multilead geometry avoids this by strongly reducing the probability amplitudes for paths from emitter to collector to traverse the ring multiple times, since with each traversal of the ring the probability increases that electrons travelling in the ring are "siphoned off" into the side arms.[32,33] We shall exploit this fact by making the assumption that *the probability amplitude for passing any side arm more than once along the way from emitter to collector is negligibly small.* This assumption amounts to reducing the problem to that of a double-slit problem, where the transmission amplitude through one arm is calculated without incorporating the effect of the other arm at all. More specifically, we mimick the multilead geometry using the following reduced "double-slit model:" The Aharonov-Bohm ring is coupled to only emitter and collector leads (as in Fig. 5, but without any side arms), i.e. α is restricted to the values 1 and 2. The effect of the side arms in the actual experiment is mimicked by taking the amplitude $t^j_{\varepsilon\alpha\sigma}$ to get from state $|j\sigma\rangle$ on the dot to state $|\varepsilon\alpha\sigma\rangle$ in lead α to be nonzero only for the *short direct* path from the dot to lead α, *without* traversing the upper arm (concretely: we take $A^L_{\varepsilon 2\sigma}=A^R_{\varepsilon 1\sigma}=0$). When calculating the current we do allow for direct paths from lead 1 to 2 via the upper arm. However, the upper arm is *ignored* for the calculation of the equilibrium local retarded or advanced Green functions $\mathcal{G}^{R/A}_{j\sigma,j'\sigma'}(E)$ using NRG. For the latter purpose, we thus use a model of a multilevel dot coupled to two independent leads, say L and R, with *equal* chemical potentials $\mu_L=\mu_R$, representing the two segments of the ring to the left and right of the ring, coupled to it by tunnelling contacts. These two segments should be treated as independent leads, due to the above double-slit assumption of ignoring the upper arm while calculating transmission through the lower arm.

With the assumptions (i) and (ii) just described, let us now obtain an expression for that part of the conductance showing Aharonov-Bohm oscillations with applied flux, $G^{AB}=\frac{\partial I_1^{AB}}{\partial V}$, where I_1^{AB} is that part of the current in lead 1 depending on $e^{i2\pi\Phi/\Phi_0}$. For the chemical potentials given by Eq. (A16), this implies that Eq. (A14) should be evaluated with $\alpha=1$, $\beta'=2$, and $\beta=1$. Using the fact that for the model of present interest spin is conserved, so that all correlators are spin-diagonal ($\mathcal{G}^{R}_{j\sigma,j'\sigma}\propto\delta_{\sigma\sigma'}$), this readily yields

$$G^{AB}(T) = \frac{e^2}{h}\sum_\sigma \int dE\ \mathrm{Re}[T_u(E)T_{d\sigma}(E)]\left(-\frac{\partial f_0(E)}{\partial E}\right). \tag{A17}$$

The amplitudes $T_{d\sigma}$ and T_u, given by

$$T_{d\sigma}(E) = \sum_{jj'} 2\pi\rho t^j_{L\sigma}\mathcal{G}^{R}_{j\sigma,j'\sigma}(E)t^{j'*}_{R\sigma}, \tag{A18}$$

$$T_u(E) = 2iA^L_{E1}S^E_{11}S^{E*}_{12}A^{R*}_{E2}, \tag{A19}$$

may be associated with the transmission of a spin-σ electron from x_L to x_R directly through the dot or once around the ring via the upper arm, respectively. (In the main text, we used a somewhat oversimplified phrasing by calling $T_{d\sigma}$ the "transmission through the lower arm including the dot" and T_u the "transmission through the upper arm.") We shall assume T_u to be energy and temperature independent, but lump with it all flux dependence, since the path associated with it essentially encircles the ring once:

$$T_u = |T_u|e^{i(2\pi\Phi/\Phi_0+\phi_0)}. \tag{A20}$$

Thus, the Aharonov-Bohm contribution to the conductance can be written in the form

$$G^{AB}(T) = \frac{e^2}{h}\sum_\sigma |T_u||t_{d\sigma}(T)|\cos\left[2\pi\frac{\Phi}{\Phi_0}+\phi_0+\alpha_\sigma(T)\right], \tag{A21}$$

where we have defined the temperature-dependent transmission amplitude for a spin-σ electron through the quantum dot by

$$t_{d\sigma}(T) = \int dE\left(-\frac{\partial f_0(E)}{\partial E}\right)T_{d\sigma}(E) \equiv |t_{d\sigma}(T)|e^{i\alpha_\sigma(T)}. \tag{A22}$$

(The T dependence enters both through that of G^R and that of f_0.) The *magnitude and phase* of $t_{d\sigma}$ can be (i) extracted via Eq. (A21) from the experimental results as well as (ii) calculated with NRG using Eqs. (A18) and (A22).

[1] A. Yacoby, M. Heiblum, D. Mahalu, and H. Shtrikman, Phys. Rev. Lett. **74**, 4047 (1995).
[2] R. Schuster, E. Buks, M. Heiblum, D. Mahalu, V. Umansky, and H. Shtrikman, Nature (London) **385**, 417 (1997).
[3] Y. Ji, M. Heiblum, D. Sprinzak, D. Mahalu, and H. Shtrikman, Science **290**, 779 (2000).
[4] Y. Ji, M. Heiblum, and H. Shtrikman, Phys. Rev. Lett. **88**, 076601 (2002).
[5] M. Avinun-Kalish, M. Heiblum, O. Zarchin, D. Mahalu, and V. Umansky, Nature (London) **436**, 529 (2005).
[6] M. Zaffalon, A. Bid, M. Heiblum, D. Mahalu, and V. Umansky, Phys. Rev. Lett. **100**, 226601 (2008).
[7] U. Gerland, J. von Delft, T. A. Costi, and Y. Oreg, Phys. Rev. Lett. **84**, 3710 (2000).
[8] P. G. Silvestrov and Y. Imry, Phys. Rev. Lett. **85**, 2565 (2000).
[9] P. G. Silvestrov and Y. Imry, Phys. Rev. B **65**, 035309 (2001).
[10] D. I. Golosov and Y. Gefen, Phys. Rev. B **74**, 205316 (2006).
[11] C. Karrasch, T. Hecht, A. Weichselbaum, Y. Oreg, J. von Delft, and V. Meden, Phys. Rev. Lett. **98**, 186802 (2007).
[12] C. Karrasch, T. Hecht, A. Weichselbaum, J. von Delft, Y. Oreg, and V. Meden, New J. Phys. **9**, 123 (2007).
[13] Y. Oreg, New J. Phys. **9**, 122 (2007).
[14] C. Bruder, R. Fazio, and H. Schoeller, Phys. Rev. Lett. **76**, 114 (1996).
[15] M. Pustilnik and L. I. Glazman, Phys. Rev. Lett. **87**, 216601 (2001).
[16] D. C. Langreth, Phys. Rev. **150**, 516 (1966).
[17] H. R. Krishna-murthy, J. W. Wilkins, and K. G. Wilson, Phys. Rev. B **21**, 1003 (1980).
[18] R. Bulla, T. A. Costi, and T. Pruschke, Rev. Mod. Phys. **80**, 395 (2008).
[19] R. Peters, T. Pruschke, and F. B. Anders, Phys. Rev. B **74**, 245114 (2006).
[20] A. Weichselbaum and J. von Delft, Phys. Rev. Lett. **99**, 076402 (2007).
[21] F. B. Anders and A. Schiller, Phys. Rev. Lett. **95**, 196801 (2005).
[22] R. Bulla, A. C. Hewson, and T. Pruschke, J. Phys.: Condens. Matter **10**, 8365 (1998).
[23] F. D. M. Haldane, Phys. Rev. Lett. **40**, 416 (1978).
[24] P. G. Silvestrov and Y. Imry, Phys. Rev. Lett. **90**, 106602 (2003).
[25] Y. Oreg and Y. Gefen, Phys. Rev. B **55**, 13726 (1997).
[26] A. Levy Yeyati and M. Büttiker, Phys. Rev. B **52**, R14360 (1995).
[27] G. Hackenbroich, Phys. Rep. **343**, 463 (2001).
[28] M. Büttiker, Phys. Rev. B **46**, 12485 (1992).
[29] J. Rammer and H. Smith, Rev. Mod. Phys. **58**, 323 (1986).
[30] M. Büttiker, A. Prêtre, and H. Thomas, Phys. Rev. Lett. **70**, 4114 (1993).
[31] M. Büttiker, Phys. Rev. Lett. **57**, 1761 (1986).
[32] A. Aharony, O. Entin-Wohlman, B. I. Halperin, and Y. Imry, Phys. Rev. B **66**, 115311 (2002).
[33] J. König and Y. Gefen, Phys. Rev. B **65**, 045316 (2002).
[34] The experiment in Ref. 2 was actually done using choices for μ_1 and μ_2 slightly different from Eq. (A16), using an "open circuit" where $\mu_1 = eV$ and μ_2 is adjusted such that no current flows into the collector.[2] The measured Aharonov-Bohm conductance will thus differ from the G^{AB} obtained using Eq. (A16) by constant prefactors, independent of V_g and T, involving ratios of the transmission probabilities at emittor and collector, discussed in Ref. 2.